Supplemental material

Purcell-enhanced spontaneous emission of molecular vibrations

Bernd Metzger,[1] Eric Muller,[1] Jun Nishida,[1] Benjamin Pollard,[1] Mario Hentschel,[2] and Markus B. Raschke[1,*]

[1]*Department of Physics, Department of Chemistry, and JILA, University of Colorado at Boulder, 2000 Colorado Ave, Boulder, CO 80309, USA*

[2]*4^{th} Physics Institute and Research Center SCoPE, University of Stuttgart, Pfaffenwaldring 57, 70569 Stuttgart, Germany*

(Dated: August 22, 2019)

Methods

Sample fabrication. The IR gold antenna arrays are defined on a CaF_2-substrate using electron beam lithography following electron beam evaporation of a 2 nm chromium adhesion layer and a 100 nm layer of gold. The nominal width of the IR antennas is 200 nm. The antenna length is varied from 1.3 µm to 2.1 µm, in a step size of nominally 100 nm. The lattice constant is 4 µm. Subsequently, we spin-coated a $\sim$ 10 nm layer of poly(methyl methacrylate) (PMMA) using a 0.5 wt% solution of PMMA in toluene.

Far-field sample characterization. Far-field reflection spectra of the IR antenna arrays (Figure 2a) are measured using a Nicolet Fourier Transform Infrared (FTIR) spectrometer system coupled to an IR microscope (Thermo Fisher Scientific).

Broadband mid-infrared laser source. We use $\sim$ 150 fs mid-IR laser pulses generated by optical parametric and difference frequency generation. A pump laser, Yb:KGW oscillator, $\sim$ 76 MHz repetition rate, with pulse energies of $>$ 75 nJ, corresponding to $>$ 6 W average power, and pulse duration of $<$ 100 fs (FLINT, Light conversion), pumps a fan-out periodically-poled lithium niobate (PPLN) optical parametric oscillator (OPO) (Levante, APE Berlin). Subsequently, difference frequency generation (DFG) between the OPO signal and idler pulses in a $AgGaS_2$ crystal generates $>$ 15 mW average power IR light tunable from $<$ 5 µm to $>$ 10 µm wavelength with a full-width half-maximum bandwidth of about 100 cm^{-1} (HarmoniXX, APE Berlin).

IR *s*-SNOM setup. For near-field optical microscopy we use a modified commercial atomic force microscope (nanoIR2s prototype, Anasys/Bruker) with gold coated tapping mode AFM probes with a cantilever resonance frequency of $\sim$ 300 kHz (160AC-GG-24, MikroMasch). For heterodyne signal detection and amplification we use an asymmetric Michelson interferometer, as described previously [1–6], with a wedged and coated 50:50 6 mm thick BaF_2 beam splitter. To compensate for the dispersion of the beam splitter the reference arm additionally contains an identical but uncoated BaF_2 substrate. The IR laser pulses are focused onto the apex region of the AFM tip using an off-axis parabolic mirror (NA = 0.45). The scattered IR light is collected in collinear backscattering, and detected with a mercury cadmium telluride (MCT) detector (KLD-0.5-J1/11, Kolmar Technolgies). For far-field background suppression we demodulate the tip-scattered signals at the second-harmonic of the cantilever tapping frequency $2\omega_c$ using lock-in detection (HF2LI, Zurich Instruments), allowing for a diffraction-unlimited spatial IR resolution down to $\sim$ 10 nm. The Michelson interferometer provides heterodyne signal detection and ampli-

fication of the tip-scattered near-field E_{nf} with the reference field $E_{\text{ref}}(\tau)$. The resulting asymmetric interferogram with free induction decay (FID) of the near-field response contains to first order the Fourier transformation analogue of the nanoscale dispersion and absorption [1–6].

Time-domain interferometry and Fourier transform nano spectroscopy. To measure the free induction decay of small molecular ensembles, the end mirror of the reference arm is mounted onto a high precision delay stage (ANT95-50-L-MP, Aerotech) and translated over a distance of 500 µm, corresponding to a temporal window of $\sim$ 3.3 ps and a spectral resolution of $\sim$ 10 cm^{-1}. For the spatio-spectral scan shown in Figure 2b of the manuscript, the interferograms are measured at a fast speed of 200 µm/s of the delay stage, to reduce sample drift during the acquisition, for a measurement time of 2.5 s per interferogram. For the precise measurements at the antenna terminals the interferograms are measured at a speed of 5 µm/s, and the interferograms are additionally averaged over 5 consecutive scans, resulting in a significantly improved signal-to-noise ratio. While the analysis of the IR *s*-SNOM signal was done directly in the time domain, the observed interferogram can be Fourier transformed to yield real (dispersive) and imaginary (absorptive) terms of the vibrational response. For the PMMA coated on the resonant antenna, the absorptive band exhibits a broadened linewidth due to the accelerated relaxation induced by the antenna-molecule coupling (Fig. 3c). Fig. S1 shows corresponding spectral signals for PMMA on a non-resonant antenna (data from FID from Fig. 3a), with a narrower linewidth due to the weaker antenna-molecule coupling and corresponding slower relaxation.

Spatio-spectral imaging. For spatio-spectral imaging, a high-resolution AFM and IR *s*-SNOM scan with an area of 2.5x1 μm^2 over the cross-section of a single IR antenna is first acquired. Subsequently, we define a rectangular evenly spaced grid with a lateral spacing of 62.5 nm over the previously measured area. Lastly, interferograms $I(\tau)$ are measured with the near-field tip positioned at each location of the predefined grid.

Model

Free induction decay fit function. As outlined in the manuscript we describe the heterodyne term of the FID signal $I_{\text{FID}}(\tau)$ by

$$I_{\text{FID}}(\tau) \propto \int_{-\infty}^{+\infty} E_{\text{nf}}(t) E_{\text{ref}}^{\star}(t-\tau) dt, \tag{1}$$

where E_{nf} and E_{ref} are the tip-scattered near-field and the reference field, respectively.

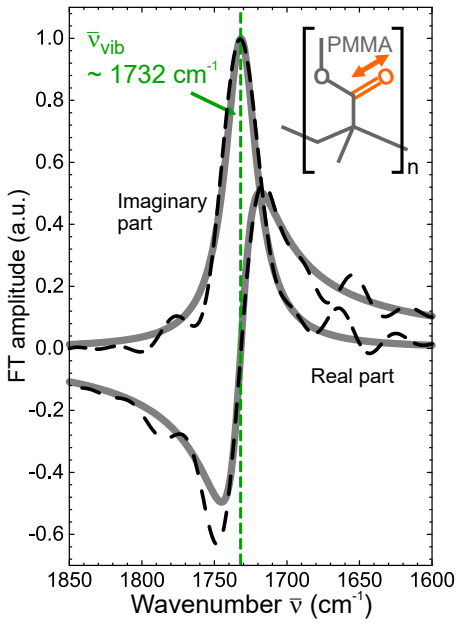

FIG. S1. The spectral real (dispersive) and imaginary (absorptive) parts of the IR *s*-SNOM response for the PMMA coated non-resonant antenna, with a narrower absorptive linewidth compared to that from the resonant antenna shown in Fig. 3c in the main text.

While E_{ref} corresponds to the incident laser field E_{in} (up to the delay τ), the tip-scattered near-field E_{nf} is modified by the antenna response $g_{\text{ant}}(t)$, as well as by the response function $\overline{g}_{\text{vib}}(t)$ of the molecular vibrations. Here, the overline in $\overline{g}_{\text{vib}}(t)$ indicates that the vibrational response does not correspond to the uncoupled response of the molecular vibrations, but that it is modified from coupling to the IR antenna. Consequently, without *a priori* knowledge of coupling we express $E_{\text{nf}}(t)$ in the time domain as a sum of two contributions as (which is only valid in the weak coupling regime)

$$\begin{aligned} E_{\text{nf}}(t) \propto & a_{\text{ant}} e^{i\phi_{\text{ant}}} \int_{-\infty}^{+\infty} g_{\text{ant}}(t-t') E_{\text{in}}(t') dt' \\ & + \overline{a}_{\text{vib}} e^{i\overline{\phi}_{\text{vib}}} \int_{-\infty}^{+\infty} \overline{g}_{\text{vib}}(t-t') E_{\text{in}}(t') dt', \end{aligned} \tag{2}$$

where we additionally accounted for the different amplitudes a_{ant} and $\overline{a}_{\text{vib}}$ and phases ϕ_{ant} and $\overline{\phi}_{\text{vib}}$ of the antenna and the molecular response, respectively.

The antenna response function $g_{\text{ant}}(t)$ is assumed instantaneous, i.e., a delta function $\delta(t)$, since the few-femtosecond Drude and radiative lifetimes are much shorter than the laser pulse duration,

and in the spectral domain the antenna response varies only negligibly over the bandwidth of our laser spectrum. Furthermore, a small additional term describes a linear frequency dependence of the antenna response at the laser center frequency ω_0

$$g_{\text{ant}}(t) = a\delta(t) + i\frac{b}{\omega_0}e^{-i\omega_0 t}\frac{d\delta(t)}{dt} \tag{3}$$

$$= \mathcal{F}\left\{a + b\frac{\omega-\omega_0}{\omega_0}\right\}, \tag{4}$$

with the parameters a and b accounting for the strength and the linear slope of the antenna response close to the laser center frequency ω_0.

The response of the molecular vibrations $\overline{g}_{\text{vib}}(t)$ is modeled as a harmonic oscillator with resonance frequency $\overline{\omega}'_{\text{vib}}$ and dephasing time $\overline{T}_{2,\text{vib}}$:

$$\overline{g}_{\text{vib}}(t) = \frac{i}{2\overline{\omega}'_{\text{vib}}} \cdot \mathrm{e}^{-t/\overline{T}_{2,\text{vib}}} \cdot \mathrm{e}^{-i\overline{\omega}'_{\text{vib}}t} \cdot \theta(t) \tag{5}$$

$$= \mathcal{F}\left\{-\frac{1}{2\overline{\omega}'_{\text{vib}}}\frac{1}{\omega - \overline{\omega}'_{\text{vib}} + i/\overline{T}_{2,\text{vib}}}\right\}, \tag{6}$$

with $\theta(t)$ being the Heaviside distribution.

Coupled oscillator model. In order to separate the different relaxation pathways of the molecular vibrations and to describe the enhanced radiative decay quantitatively, we model the combined behavior for antenna and molecules as coupled harmonic oscillators:

$$\ddot{x}_{\text{ant}} + 2/T_{2,\text{ant}}\dot{x}_{\text{ant}} + \omega_{\text{ant}}^2 x_{\text{ant}} - \kappa x_{\text{vib}} = qE_{\text{in}}(t) \tag{7}$$

$$\ddot{x}_{\text{vib}} + 2/T_{2,\text{vib}}\dot{x}_{\text{vib}} + \omega_{\text{vib}}^2 x_{\text{vib}} - \kappa x_{\text{ant}} = 0 \tag{8}$$

Here, $x_{\text{ant}}(t)$ and $x_{\text{vib}}(t)$ are the effective oscillator amplitudes of the antenna and the molecules, $T_{2,\text{ant}}$ and $T_{2,\text{vib}}$ are the uncoupled dephasing times, ω_{ant} and ω_{vib} are the uncoupled resonance frequencies, q describes the excitation coupling strength of the IR antenna, κ is a coupling constant, and $E_{\text{in}}(t)$ is the incident driving field.

A Fourier transform turns the coupled differential equations into a system of linear equations

$$\underbrace{\begin{pmatrix} 1/g_{\text{ant}}(\omega) & -\kappa \\ -\kappa & 1/g_{\text{vib}}(\omega) \end{pmatrix}}_{\underline{\underline{M}}} \begin{pmatrix} x_{\text{ant}}(\omega) \\ x_{\text{vib}}(\omega) \end{pmatrix} = \begin{pmatrix} q \\ 0 \end{pmatrix} E_{\text{in}}(\omega), \tag{9}$$

with

$$g_j(\omega) = -\frac{1}{\omega^2 - \omega_j^2 + 2i\omega/T_{2,j}} \qquad (j = \text{ant, vib}) \tag{10}$$

$$\approx -\frac{1}{2\omega_j'}\frac{1}{\omega - \omega_j' + i/T_{2,j}}, \tag{11}$$

which are the linear response functions of the individual oscillators, and the ω_j's are the red-shifted near-field resonance frequencies, with $\omega_j'^2 = \omega_j^2 - 1/T_{2,j}^2$.

After diagonalizing the matrix $\underline{\underline{M}}$, and assuming that the coupling is weak, i.e, the coupled response functions $\overline{g}_{\text{ant}}(\omega)$ and $\overline{g}_{\text{vib}}(\omega)$ still exhibit Lorentzian form as described by equation (11), we obtain new eigenfrequencies $\overline{\omega}'_{\text{ant}}$ and $\overline{\omega}'_{\text{vib}}$ and modified dephasing times $\overline{T}_{2,\text{ant}}$ and $\overline{T}_{2,\text{vib}}$. For the molecular vibrations the calculation yields

$$\overline{\omega}'_{\text{vib}} = \omega'_{\text{vib}} + \frac{\kappa^2}{4\omega'_{\text{ant}}\omega'_{\text{vib}}}\frac{\Delta\omega'}{\Delta\omega'^2 + \Delta\Gamma^2}, \tag{12}$$

$$\frac{1}{\overline{T}_{2,\text{vib}}} = \frac{1}{T_{2,\text{vib}}} - \frac{\kappa^2}{4\omega'_{\text{ant}}\omega'_{\text{vib}}}\frac{\Delta\Gamma}{\Delta\omega'^2 + \Delta\Gamma^2}, \tag{13}$$

where $\Delta\Gamma = 1/T_{2,\text{vib}} - 1/T_{2,\text{ant}}$ and $\Delta\omega' = \omega'_{\text{vib}} - \omega'_{\text{ant}}$ correspond to the difference in the dephasing rates and to the detuning.

In order to obtain quantitative expressions for the amplitude and the phase of the molecular vibrations, we invert the oscillator matrix $\underline{\underline{M}}$ from equation (9). This yields a solution for the antenna amplitude $x_{\text{ant}}(\omega)$

$$x_{\text{ant}}(\omega) = -\frac{g_{\text{ant}}}{1 - \kappa^2 g_{\text{ant}} g_{\text{vib}}} q E_{\text{in}}(\omega) \tag{14}$$

$$\approx -q\left(g_{\text{ant}} + \kappa^2 g_{\text{ant}}^2 g_{\text{vib}}\right) E_{\text{in}}(\omega), \tag{15}$$

where we again assumed that coupling between the antenna and the molecules is in the weak coupling regime.

We then assume that the tip scattered near-field $E_{\text{nf}}(\omega)$ is proportional to the antenna oscillator amplitude $x_{\text{ant}}(\omega)$, and after comparison of equation (15) with a Fourier transform of equation (2) we find to a good approximation for the vibrational amplitude $\tilde{a}_{\text{vib}}$ and for the associated phase $\Delta\phi$ of the molecular signals

$$\widetilde{a}_{\text{vib}} \sim \kappa^2 \frac{T_{2,\text{vib}}}{\overline{T}_{2,\text{vib}}} \left|g_{\text{ant}}(\omega_0)\right|, \tag{16}$$

$$\Delta\phi \sim -2 \cdot \arctan\left(\frac{1/T_{2,\text{ant}}}{\omega_0 - \omega'_{\text{ant}}}\right), \tag{17}$$

where $g_{\text{ant}}(\omega_0) = -\{(2\omega'_{\text{ant}})(\omega_0 - \omega'_{\text{ant}} + i/T_{2,\text{ant}})\}^{-1}$ corresponds to the amplitude of the IR antenna at the laser center frequency ω_0. The equations (13), (16), and (17) for the dephasing time $\overline{T}_{2,\text{vib}}$, the vibrational amplitude $\widetilde{a}_{\text{vib}}$ and phase $\Delta\phi$ are then used to describe the corresponding measured quantities. The resulting fits are displayed in Figure 4 of the manuscript together with the measurement, and are found to be in good agreement.

* markus.raschke@colorado.edu

[1] S. Amarie, T. Ganz, and F. Keilmann, Opt. Express **17**, 21794 (2009).

[2] M. Schnell, A. Garcia-Etxarri, A. J. Huber, K. B. Crozier, A. Borisov, J. Aizpurua, and R. Hillenbrand, The Journal of Physical Chemistry C **114**, 7341 (2010).

[3] X. G. Xu, M. Rang, I. M. Craig, and M. B. Raschke, The Journal of Physical Chemistry Letters **3**, 1836 (2012).

[4] F. Huth, A. Govyadinov, S. Amarie, W. Nuansing, F. Keilmann, and R. Hillenbrand, Nano Letters **12**, 3973 (2012).

[5] I. Amenabar, S. Poly, W. Nuansing, E. H. Hubrich, A. A. Govyadinov, F. Huth, R. Krutokhvostov, L. Zhang, M. Knez, J. Heberle, A. M. Bittner, and R. Hillenbrand, Nat Commun **4**, 2890 (2013).

[6] E. A. Muller, B. Pollard, and M. B. Raschke, J Phys Chem Lett **6**, 1275 (2015).